

## Numerical Study on Low Speed Electric Car for Public Transportation to Predict its Aerodynamic Performance and Stability

Tatek Mamo<sup>1</sup>, Rajendran Gopal<sup>2</sup>, Bisrat Yoseph<sup>3</sup>, Samuel Tamirat<sup>4</sup>, Yared seifu<sup>5</sup>

<sup>1,4,5</sup>Adama Science and Technology University, Adama, Ethiopia

<sup>2,3</sup>EFDRE Defense Engineering College Department of Motor Vehicle, Bishoftu, Ethiopia

**ABSTRACT:** Energy efficiency and dynamic stability of Battery Electric Vehicle (BEV) is highly influenced by size of powertrain, aerodynamic characteristics and driving conditions. The main idea of this work was to study aerodynamic performance of BEV sized based on Ethiopian driving profile and BAJAJ QUTE chassis platform. Numerical analysis was conducted to reveal various surface features and side wind velocities influence using coefficients of aerodynamic forces and moments, vector and contour plots of CFD (Computational Fluid Dynamics). From the analysis, it was found that average aerodynamic coefficients and moments with side wind are much higher than simulated values of original car with corresponding values of CD (3.11), CL (0.45), YM (-240.52Nm) and RM (-363.84Nm). The power requirement to overcome aerodynamic road load with 10m/sec side wind has increased (13.36kW) by 3.3 times as compared to no wind effect power of (4.05kW). The car moving through a straight level road found to be stable at any side-wind below 15m/sec, but it could reach to unstable condition in curved road. For car moving in any road under side-wind greater than 15m/s, there is a chance of turnover and breakaway of a lane.

**KEYWORDS:** Aerodynamic moment, BEV, drag coefficient, lift coefficient, CFD, stability

### 1. INTRODUCTION

In recent decades, emphasis is given for adoption of BEVs to improve energy efficiency while reducing environmental pollution. Currently Most Original Equipment Manufacturers (OEM) have been shifting to BEVs and different type with improved ranges are available [1, 2]. However, their market penetration is lagging behind as long range vehicles require heavy battery and new platform. On the other hand adopting conversion design on largely evolved automotive body and chassis architecture has not addressed to offer lower costs and short time-to-market [3]. Especially for developing countries like Ethiopia, where abundant electricity potential is available could be more valuable. Ethiopia is favoured by estimated hydropower potential 45,000 MW and currently mega projects are under construction. This approach could generate a lot of interest and necessitates a comprehensive analysis and development to put forth new and efficient technologies [4, 5].

In conversion approach placement of EV drive train components was based on space available and battery pack is along the floor of the vehicle. Due to shift of powertrain location and geometry modification BEVs involve significant change in axle weight distribution and they are highly exposed to aerodynamic drag and lift forces [6]. The aerodynamic drag force is road load consumes power and lift tendency highly influences stability even at lower speeds, when gust side wind happen. Substantial effort and

continuous work towards improving the aerodynamic performance and increasing range of electric vehicles have been done. However, study on low speed aerodynamics is mainly ignored, where its influence is significant even for small side wind[7].

In this work low speed electric car for public transportation was studied to predict its aerodynamic performance addressing the effect on power consumption and stability. The car selected is BAJAJ QUTE, one of Indian product widely used for urban public transport and considered to be suitable for most developing countries [8-10]. The battery size is significant factor and influenced by driving profile and no reports are available to estimate according to Ethiopian routes. Hence, GPS based data was collected to address all possible geographical states the vehicle population can trace in Addis Ababa and sub urban routes of 60Km radius. Components of powertrain were sized based up on performance requirements of typical driving profile. The existing rear drive arrangement was used to place motor and transmission, whereas battery pack and controllers loaded along floor of passenger compartment. The CAD model of the car was developed by using Catia-v5 software with same dimension, imported to Phonics CFD domain and numerical grid generated the in the rectangular coordinate system. Calculations were conducted in optimized grid distribution obtained by thorough grid dependence evaluation and converged with an error cut off less than 0.01%. The

## “Numerical Study on Low Speed Electric Car for Public Transportation to Predict its Aerodynamic Performance and Stability”

aerodynamic characteristics when the car is moving at top speed (70km/h) by varying side wind cases at 0m/sec, 10m/sec, 20m/sec, 30m/sec and 40m/sec were examined numerically.

### 2. AERODYNAMIC CHARACTERISTICS OF A CAR BODY

When the vehicle is moving at a considerable speed, the air passing over it imposes various forces and moment on the vehicle [11]. The essential coefficients of aerodynamic force and moments can be calculated by the following analytical relations.

$$C_L = \frac{F_L}{\frac{1}{2}\rho(V_\infty - V)^2 A} \quad (1)$$

$$C_D = \frac{F_D}{\frac{1}{2}\rho(V_\infty - V)^2 A} \quad (2)$$

$$C_S = \frac{F_S}{\frac{1}{2}\rho V^2 A} \quad (3)$$

$$C_{RM} = \frac{R_M}{\frac{1}{2}\rho(V_\infty - V)^2 At} \quad (4)$$

$$C_{YM} = \frac{Y_M}{\frac{1}{2}\rho(V_\infty - V)^2 At} \quad (5)$$

$$C_{PM} = \frac{P_M}{\frac{1}{2}\rho(V_\infty - V)^2 At} \quad (6)$$

Where; (CL = Lift Coefficient, FL = Lift force, CD = Drag Coefficient, FD = Drag force, CS = Side force coefficient, FS = Side force, CRM = Rolling moment coefficient, RM = Rolling moment, CYM = Yawing moment coefficient, YM = Yawing moment, CPM = Pitching moment coefficient, PM = Pitching moment, V∞ = Free stream velocity, V = Total wind velocity, A = Projected frontal area, t = reference length may be taken t=L= Wheelbase).

### 3. MODELING AND NUMERICAL SCHEME DEFINITION

#### 3.1 CAD MODEL AND GEOMETRY OF THE CAR

The model car (QUTE) is one of general models of low speed hatchback, which dimensions and technical specifications along with CAD model are presented on Table 1 and Figure 1.

**Table 1. Technical specification of model car (Bajaj QUTE)**

| Parameters                     | Value                         |
|--------------------------------|-------------------------------|
| Peak Power                     | 9.9 Kw @ 5500 (Kw @ RPM)      |
| Maximum Torque                 | 19.6 @ 4000 (Nm @ RPM)        |
| Number of Passengers           | 4 (75Kg/person)               |
| Glider Weight                  | 400Kg                         |
| Battery and controllers Weight | 70Kg                          |
| Motor and transmission         | 30Kg                          |
| Gross weight                   | 800Kg                         |
| Max. Speed                     | 70km/h                        |
| CD                             | 0.45                          |
| CL                             | 0.035                         |
| C.G coordinate (X, Y, Z)       | ( 1.4,0.65, 0.8)              |
| Projected total area           | 0.85×h×w =1.823m <sup>2</sup> |



**Figure 1. Exterior overall dimensions (a) and CAD model (b) of BAJAJ QUTE**

#### 3.2 NUMERICAL SCHEME

FVM (Finite Volume Method) scheme was employed to simulate flow phenomenon by considering side wind effect at 0m/sec, 10m/sec, 20m/sec, 30m/sec and 40m/sec. Numerical investigations have been conducted with PHOENICS

program for the same conditions to simulate and solve equations of flow around the model vehicles. The general purpose CFD was used for a numerical calculation of the turbulent incompressible flow field. 3-D dimensional Navier-

# “Numerical Study on Low Speed Electric Car for Public Transportation to Predict its Aerodynamic Performance and Stability”

Stokes equations were solved with standard (K-ε) turbulent model.[12]

### 3.2.1 Numerical domain and grid

The CAD-to-CFD method and orthogonal grids was incorporated for the numerical grid formation. The CAD model imported to the numerical domain to generate the numerical grid in the rectangular coordinate system. The

numerical size of domain in (X, Y, Z) is defined as (22m, 6.8m, and 5.5m). The calculation was conducted at optimized grid distribution shown in Figure 5, which is obtained by thorough grid dependence evaluation with different iterations and very nicely converged with an error cut off less than 0.01%.

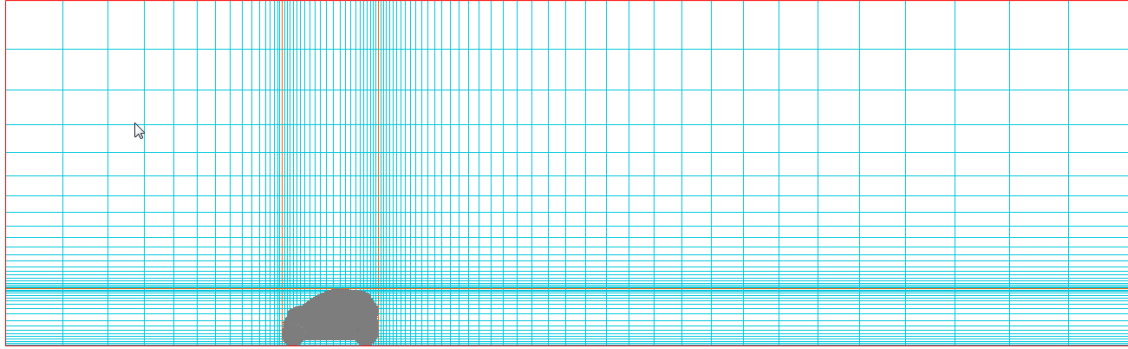


**Figure 2. Optimized computational grid of model car (47x94x41)**

In the developed boundary conditions the flow type was assumed as turbulent, transient and incompressible and subjected to suitable boundary condition for vehicle body aerodynamic parameters. The initial and boundary conditions are defined as given in the Table 2.

**Table 2. Implemented boundary and initial conditions**

| Boundary surface      | Boundary & initial conditions                     |
|-----------------------|---|
| Inlet-one             | Longitudinal Velocity inlet (70 km/h)             |
| Left side (Inlet-two) | Side wind Velocity inlet (0, 10, 20, 30, 40m/sec) |
| Outlet                | Pressure outlet                                   |
| Right Side and top    | No slip wall condition                            |
| Ground                | moving ground type                                |
| Flow domain           | Quasi-3D flow, Turbulent and incompressible flow  |

### 3.2.2 Numerical domain and grid

The basic equations of fluid dynamics in the control volume are based on Navier stokes equations that are comprised of equation for conservation of mass and momentum are given as,[13]

#### 1. Continuity equation

$$\frac{\partial U_i}{\partial x_i} + \frac{\partial U_j}{\partial y_j} + \frac{\partial U_k}{\partial z_k} = 0 \quad (7)$$

#### 2. Momentum equation`

$$\frac{\partial U_i}{\partial t} + \frac{\partial}{\partial x_j} (U_j U_i) = -\frac{1}{\rho} \frac{\partial P}{\partial x_i} + \frac{\partial}{\partial x_j} \left[ \nu \left( \frac{\partial U_i}{\partial x_j} + \frac{\partial U_j}{\partial x_i} \right) \right] - u_i g_i \quad (8)$$

Where;  $\overline{-U_i U_j} = \nu_t \left[ \left( \frac{\partial U_i}{\partial x_j} + \frac{\partial U_j}{\partial x_i} \right) \right] - \frac{2}{3} k \sigma_{ij}$

#### 3. Standard κ-ε turbulent model; turbulent kinetic energy equation

$$\frac{\partial}{\partial x_i} (U_j k) = \frac{\partial}{\partial x_j} \left[ \nu \left( v + \frac{\nu_t}{\sigma_k} \right) \frac{\partial k}{\partial x_j} \right] + G - \varepsilon \quad (9)$$

#### 4. Energy dissipation equation

$$\frac{\partial}{\partial x_i} (U_j \varepsilon) = \frac{\partial}{\partial x_j} \left[ \nu \left( v + \frac{\nu_t}{\sigma_\varepsilon} \right) \frac{\partial \varepsilon}{\partial x_j} \right] + \frac{\varepsilon}{k} (C_{\varepsilon 1} G - C_{\varepsilon 2} \varepsilon) \quad (10)$$

$$G = \overline{-U_i U_j} = \left[ \left( \frac{\partial U_i}{\partial x_j} \right) \right] \text{ (Production rate due to deformation)}$$

$$\nu_t = C_\mu \frac{k^2}{\varepsilon}$$

$$(C_\varepsilon = 0.09, C_{\varepsilon 1} = 1.44, C_{\varepsilon 2} = 1.92, \sigma_k = 1.0, \sigma_\varepsilon = 1.0)$$

k- turbulent energy, ε-dissipation rate, ν<sub>t</sub> & ν<sub>t</sub> laminar and turbulent kinematic viscosities[14-16].

## 4. RESULTS AND DISCUSSIONS

### 4.1 QUANTITATIVE ANALYSIS

Closely examining the CFD simulation result in Figure 3(a), linear increase in C<sub>D</sub> with side wind speed was indicated. The simulated average C<sub>D</sub> value of 3.11 was observed to be very high as compared to original car specification 0.45. At no wind effect case also the C<sub>D</sub> value of model car 0.54 is slightly higher than original car value.

# “Numerical Study on Low Speed Electric Car for Public Transportation to Predict its Aerodynamic Performance and Stability”

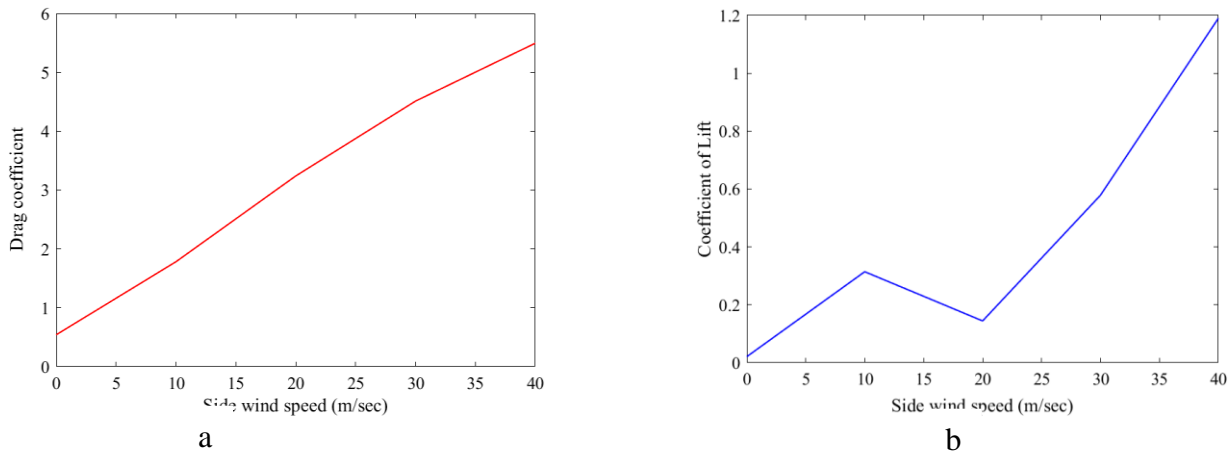


**Figure 3. Variation of  $C_D$  (a) and  $C_L$  (b) value of model car with different side wind velocity**

Figure 3(b) shows aerodynamic lift variation with side wind speed, where it linearly increases for higher side wind velocities. However, for 0 side wind velocity the  $C_L$  value of model car 0.02 is lower than original car 0.035. At 10m/sec side wind higher  $C_L$  (0.31) and  $C_D$  (1.78) values were

observed as compared to 20m/sec. This could be due to form drag and the tendency of model to uplift as a result of the decrease in under body opposite to wind side flow velocity. The increase in drag found to consume 3.3 times higher power as compared to no side wind effect case. At this speed the car is prone uplift and it will tend to be unstable.

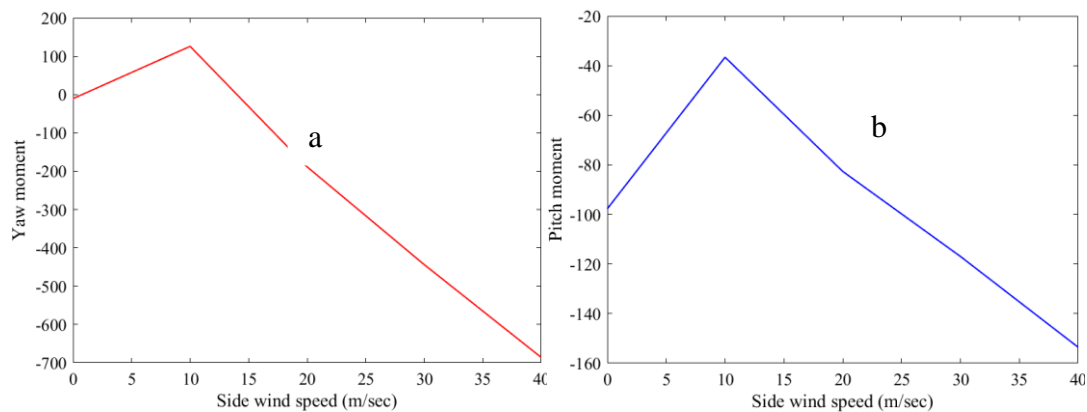


**Figure 4. Variation of induced yaw (a) and pitch moment (b) with side wind speed**

The simulated results indicated that there is paramount linear increase for all induced moments with side wind. As shown in Figure 4(a) and (b) negative sign on Yaw (-240.52Nm) and roll (-363.84Nm) moment indicates the vehicle tends to be un-stable and move outward of the road. Roll moments is more dangerous for the specific model specially cornering and moving on banking road of higher than  $4^\circ$ . The average pitch moment (-97.50Nm) is similar to no wide effect case,

but at 10m/sec it is found to be -36.61Nm and the car tend to loose traction due to uplift effect.

## 4.2 QUALITATIVE ANALYSIS

### 4.2.1 Distribution of Velocity vector

Aerodynamic characteristics was analysed qualitatively from velocity vector plot and countour plot for pressure and kinetic energy. Vector plots effectively show the differences in the velocity of the airflow over certain sections of the car's body

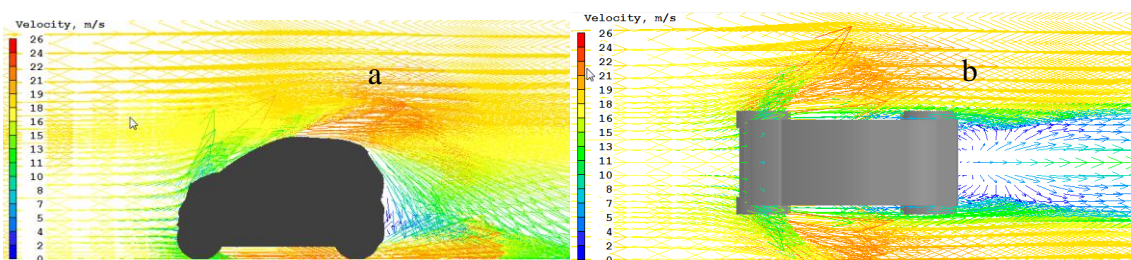


**Figure 5. Distribution of side (a) and top (b) view velocity vectors around model car with 0m/sec side wind velocity**

## “Numerical Study on Low Speed Electric Car for Public Transportation to Predict its Aerodynamic Performance and Stability”

As shown in the Figures 5(a) and (b) that the high velocity flow regions are around the transition of the windshield to the roof, the rear windshield transition, under body and just after the nose of the car at no side wind simulation.

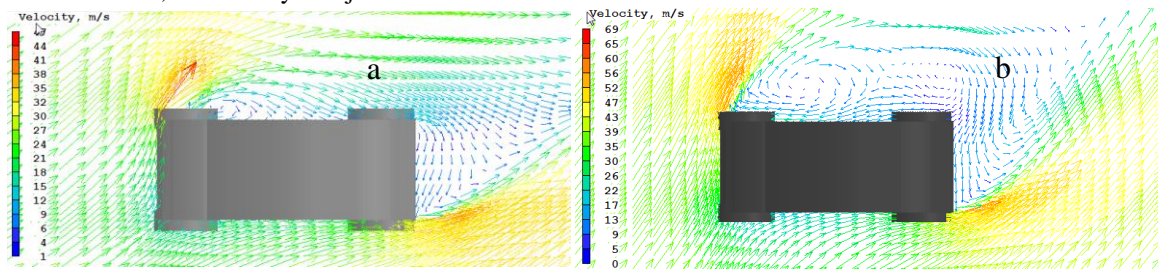


**Figure 6. Distribution of velocity vectors around model car with 10m/sec (a) and 20m/sec (b) side wind velocity**

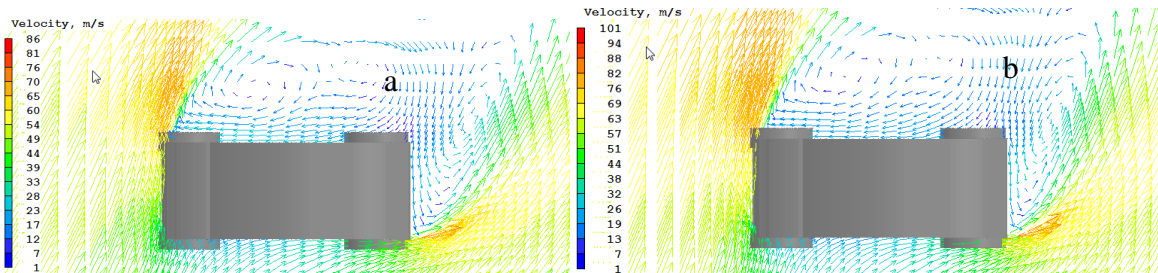


**Figure 7. Distribution of velocity vectors around model car with 30m/sec (a) and 40m/sec (b) side wind velocity**

Low velocity was observed around front bumper, wheel arc, side walls and wake region. Rear region, where streamlines detach due to square back nature of original car was found to be most critical to form wake drag.

Figures 6 and 7 compares the distribution streamwise velocity component (vectors) around the whole body surface of model car at different side wind velocities of 10, 20, 30 and 40m/sec. The result obtained from simulation with wind effect has shown low air flow velocity around the vehicle viewed on

wind flow side. But higher velocity vector is observed at right front and rear left corners of the vehicle. This disturbed air flow tends to yaw the vehicle about vertical (z-axis) and the driver loose steering controlability.

### 4.2.2 Variation of pressure contour

Figures 8 (a) and (b) shows aerodynamic pressure coefficient ( $C_p$ ) variation of model car moving at constant speed of 27.78m/sec with no side wind effect.

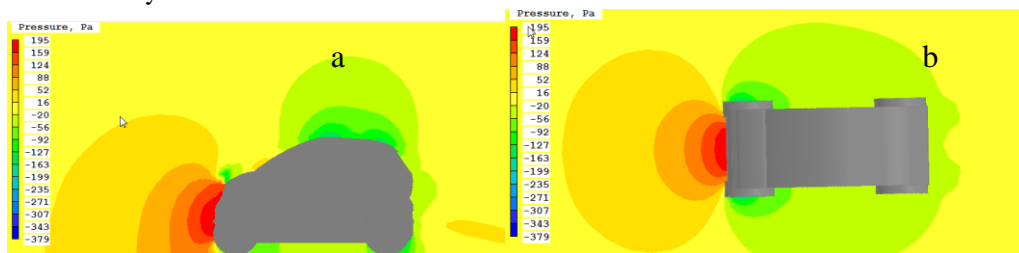


**Figure 8. Side (a) and top (b) view Pressure contour plot with no side wind effect**

High pressure is resulted at fore end of the vehicle when there is no side wind effect due to high stagnation pressure. The flow at the upper body separated near the trailing edge of the roof and high pressure reduction and wake is formed at the

rear end. In this simulation the effect of skin friction is insignificant and dominated by high difference in pressure of front and rear. As a result high form drag is resulted around the body of the vehicle.

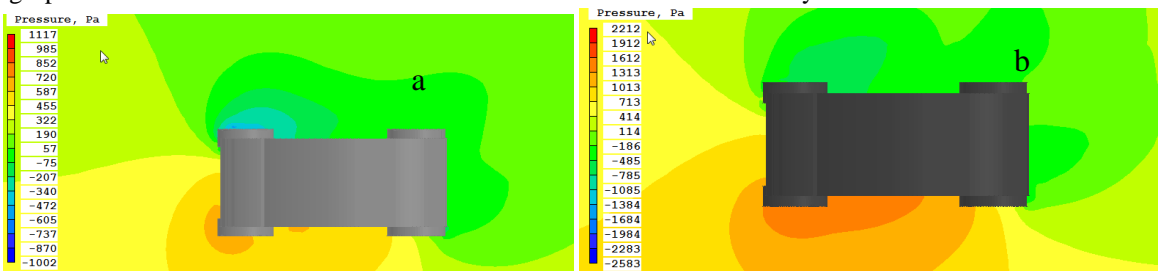


**Figure 9. The effect of side wind velocity 10m/sec (a) 20m/sec (b) on aerodynamic pressure coefficient of model car moving at constant speed of 27.78m/sec**

# “Numerical Study on Low Speed Electric Car for Public Transportation to Predict its Aerodynamic Performance and Stability”

The effect of side wind velocity on aerodynamic pressure coefficient ( $C_p$ ) was presented in Figures 9 and 10. As side wind velocity increases, the fore end stagnation pressure and wake formed at rear end of vehicle decreases drastically. But

pressure reduced on rear, underside opposite side of a car to wind flow direction due to generated eddies. Hence overall drag force around the vehicle body increased due to pressure difference on both sides of the vehicle.

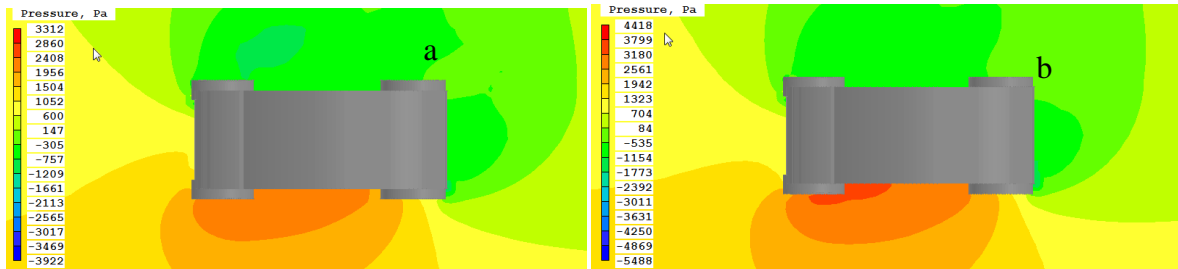


Figure 10. The effect of side wind velocity 30m/sec (a) 40m/sec (b) on pressure coefficient

### 4.2.3 Variation of turbulent kinetic energy contour

Figure 11 (a) and (b) shows aerodynamic turbulent kinetic energy of model car moving at constant speed of 27.78m/sec. High turbulent kinetic energy generated at front, over the roof and rear side of vehicle when there is no side wind effect. The rear of the model car was found to be dominant due to the induced eddy around wake region, contributes significantly in the formation of form drag.

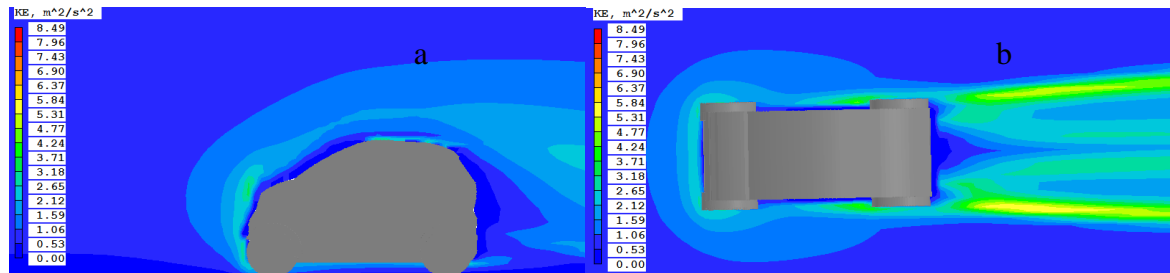


Figure 11. Turbulent kinetic energy contour at side (a) and top (b) view with no side wind

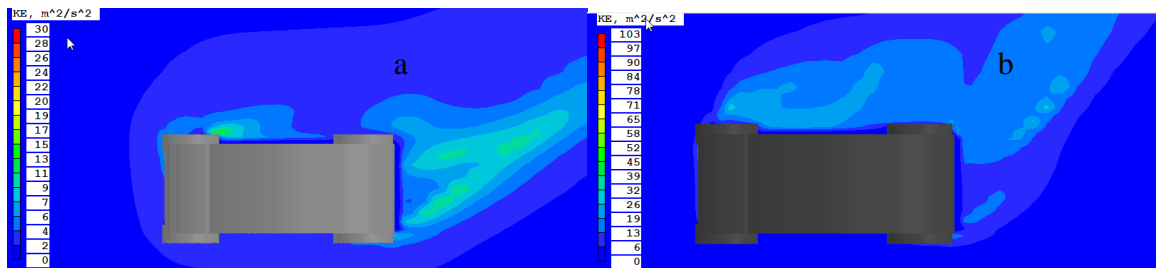


Figure 12. Effect of 10m/sec (a) and 20m/sec (b) side wind turbulent kinetic energy

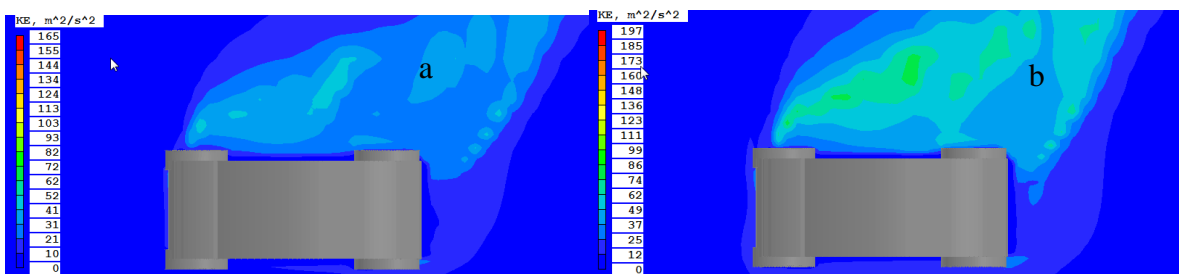


Figure 113. Effect of 30m/sec (a) and 40m/sec (b) side wind turbulent kinetic energy

Figures 12 and 13 show aerodynamic turbulent kinetic energy variation with side wind velocities for model car moving at constant speed of 27.78m/sec. Due to side wind effect

the turbulent zone mainly on opposite side to wind flow direction of vehicle.

# “Numerical Study on Low Speed Electric Car for Public Transportation to Predict its Aerodynamic Performance and Stability”

## 5. CONCLUSION

In this work aerodynamic characteristics of BEV sized based on Ethiopian driving and BAJAJ QUTE body and structure platform was studied. Typical driving cycle unique for Addis Ababa city and sub urban, which was synthesized in PhD preceding work, was utilized to determine size of powertrain. Numerical analysis on CAD model of the car was conducted to reveal influence of surface features and side wind velocities of 0, 10, 20, 30 and 40m/sec with different techniques of simulations using CFD.

From the analysis, it was found that average aerodynamic coefficients and moments are much higher than simulated values of original car with corresponding values of CD (3.11), CL (0.45), YM (-240.52Nm) and RM (-363.84Nm). The increment of drag force with side wind is due to form drag induced underbody, rear side and on opposite side of wind attack which causes vortex flow. The shape of vehicle; front panel, rear panel, under body and wheel arc zones are major causes of drag coefficients of original car model. From this study, it was found that the power requirement of model car to overcome aerodynamic road load with 10m/sec side wind has increased (13.36kW) by 3.3 times as compared to no wind effect power (4.05kW). The model car found to be under the stable condition at any side-wind below 15m/sec, while moving through a straight level road. However, as it moves through the curved road under side-wind condition, it could reach to the unstable condition dynamically. When the car moves through a curved or straight road under side-wind greater than 15m/s, there is a chance of turnover and breakaway of lane.

## ABBREVIATIONS

BEV: Electric Vehicles

$C_L$ : Lift Coefficient

CAD: Computer Aided Design

$C_D$ : Drag Coefficient

CFD: Computational Fluid Dynamics

RPM: Revolution per Minute

C.G: Centre of Gravity

K- $\epsilon$  Kinetic Energy Turbulent Model

## DATA AVAILABLE ON REQUEST

The data used for this study are available from the corresponding author upon request.

## CONFLICTS OF INTEREST

The authors declare that there are no conflicts of interest regarding the publication of this study.

## ACKNOWLEDGEMENT

The authors would like to thank Adama Science and Technology University SHEGER Addis Ababa city bus organization for

providing GPS instrumented vehicles for data collection.

## REFERENCES

1. Lander, L., et al., *Breaking it down: A techno-economic assessment of the impact of battery pack design on disassembly costs*. Applied Energy, 2023. **331**: p. 120437.
2. Kavi, A., *A Review on Electric Vehicle Powertrain System Components and the Challenges Involved in their Large-Scale Introduction*. 2022.
3. DINESH, G., *DESIGN AND STRUCTURAL ANALYSIS OF A BICYCLE FRAME UNDER STATIC LOADING CONDITIONS*. 2022, Andhra University.
4. Khan, B. and P. Singh. *The current and future states of Ethiopia's energy sector and potential for green energy: A comprehensive study*. in *International Journal of Engineering Research in Africa*. 2017. Trans Tech Publ.
5. Cramer, C. and J. Sender, *Policy, Political Economy, and Performance in Ethiopia's Coffee Sector*, in *The Oxford Handbook of the Ethiopian Economy*. 2019, Oxford University Press.
6. Kabalan, B., *Systematic methodology for generation and design of hybrid vehicle powertrains*. 2020, Université de Lyon.
7. Huluka, A.W. and C.H. Kim, *Numerical study on aerodynamic drag reduction and energy harvest for electric vehicle: a concept to extend driving range*. IOP Conference Series: Materials Science and Engineering, 2019. **700**(1): p. 012009.
8. Wang, X., J. Liu, and Y. Deng, *The Effect on Aerodynamic Performance of Electric Vehicle Caused by Battery Pack Installed in the Chassis*. DEStech Transactions on Computer Science and Engineering, 2017(icmsie).
9. Aiyana, M. and S.S. Sagar, *Design and Optimization of an Electric Car Chassis and Body Using Structural Analysis and Computational Fluid Dynamics*. 2022, SAE Technical Paper.
10. Han, B., et al., *Developing a Regional Drive Cycle Using GPS-Based Trajectory Data from Rideshare Passenger Cars: A Case of Chengdu, China*. Sustainability, 2021. **13**(4).
11. Liu, T., et al., *Driving conditions-driven energy management strategies for hybrid electric vehicles: A review*. Renewable and Sustainable Energy Reviews, 2021. **151**: p. 111521.
12. Singh, M.K., et al., *Driver behaviour modelling of vehicles at signalized intersection with heterogeneous traffic*. IATSS Research, 2022. **46**(2): p. 236-246.

## “Numerical Study on Low Speed Electric Car for Public Transportation to Predict its Aerodynamic Performance and Stability”

13. Sabater, C. and S. Görtz, *Gradient-Based Aerodynamic Robust Optimization Using the Adjoint Method and Gaussian Processes*. 2021. **55**: p. 211-226.
14. Ebrahim, H., R. Dominy, and N. Martin, *Aerodynamics of electric cars in platoon SAGE publications*. Proceedings of the Institution of Mechanical Engineers, Part D: Journal of Automobile Engineering, 2020. **235**(5): p. 1396-1408.
15. Indrojarwo, B.T., A. Estiyono, and A.R. Pratama, *Exterior Electric Hatchback Crossover Car Design with Strong, Vicious and Sharp Concept*. IOP Conference Series: Materials Science and Engineering, 2019. **588**(1): p. 012028.
16. Li, Y. and H. Zhu, *A Research on Electric Car Styling Design and Low Aerodynamic Drag*. IOP Conference Series: Materials Science and Engineering, 2019. **573**(1): p. 012014.